Available online at www.sciencedirect.com
SCIENCE DIRECT®
Journal of Theoretical Biology 227 (2004) 437–443
Journal of Theoretical Biology
www.elsevier.com/locate/jtbi

A phenomenological model for atherosclerotic plaque growth and rupture

T.I. Zohdi[a,*], G.A. Holzapfel[b], S.A. Berger[a]

[a] Department of Mechanical Engineering, University of California, 6195 Etcheverry Hall, Berkeley, CA 94720-1740, USA
[b] Institute for Structural Analysis-Computational Biomechanics, Graz University of Technology, 8010 Graz, Schiesstattgasse 14-B, Austria

Received 18 September 2003; received in revised form 19 November 2003; accepted 20 November 2003

Abstract

The objective of this communication is to develop a computer-based framework for the overall coupled phenomena leading to growth and rupture of atherosclerotic plaques. The modeling is purposely simplified to expose the dominant phenomenological controlling mechanisms, and their coupled interaction. The main ingredients of the present simplified modeling approach, describing the events that occur due to the presence and oxidation of excess low-density lipoprotein (LDL) in the intima, are: (i) adhesion of monocytes to the endothelial surface, which is controlled by the intensity of the blood flow and the adhesion molecules stimulated by the excess LDL, (ii) penetration of the monocytes into the intima and subsequent inflammation of the tissue, and (iii) rupture of the plaque accompanied with some degree of thrombus formation or even subsequent occlusive thrombosis. The set of resulting coupled equations, each modeling entirely different physical events, is solved using an iterative staggering scheme, which allows the equations to be solved in a computationally convenient decoupled fashion. Theoretical convergence properties of the scheme are given as a function of physical parameters involved. A numerical example is given to illustrate the modeling approach and an a priori prediction for time to rupture as a function of arterial geometry, diameter of the monocyte, adhesion stress, bulk modulus of the ruptured wall material, blood viscosity, flow rate and mass density of the monocytes.

Keywords: Atherosclerotic plaque; Vulnerable plaque; Plaque growth; Plaque rupture

1. Introduction

Atherosclerosis is a vascular disease associated with the accumulation of lipids leading to invasion of leukocytes (monocytes) and smooth muscle cells into the intima, a process which may proceed to the formation of atheroma. Biomechanical and biochemical mechanisms are involved in the development of the lesions characteristic of atherosclerotic plaque. Myocardial infarction and stroke can result from plaque rupture and subsequent release of highly thrombogenic material and lipids into the blood stream.

Lesions with high risk of rupture are termed *vulnerable*, (see, for example, Fuster, 2002). These lesions, culprits in the sudden life-threatening cardiovascular events, are associated with, among other features, micromorphological characteristics, such as plaque cap thickness (Richardson et al., 1989; Loree et al., 1992), and lipid core size (Davies et al., 1993). The study suggested that silent subclinical plaque rupture occurs frequently in patients with atherosclerosis. The size and bulk of lesions is likely to increase as a result of repeated sequences of rupture and repair. This may explain why myocardial infarction often occurs in asymptomatic patients. No adequate diagnostic strategy for the identification of vulnerable plaques is available yet. Investigators are striving to determine why one plaque is vulnerable and life-threatening while another one is resistant and innocuous. Elucidation of the mechanisms and factors involved in plaque initiation, growth, and development could lead to strategies to stabilize atherosclerotic plaques and to prevent plaque rupture through lesion-specific interventions (see, for example, Libby and Aikawa, 2002).

Certain aspects of the overall growth process are well understood. Essentially, excess low-density lipoprotein

*Corresponding author.
E-mail addresses: zohdi@newton.berkeley.edu (T.I. Zohdi), gh@biomech.tu-graz.ac.at (G.A. Holzapfel), saberger@me.berkeley.edu (S.A. Berger).

0022-5193/$ - see front matter © 2003 Elsevier Ltd. All rights reserved.
doi:10.1016/j.jtbi.2003.11.025

(LDL) particles accumulate in the intima inducing a series of biochemical events, which cause endothelial cells to produce cell adhesion molecules, which latch onto blood monocytes. In the intima, the monocytes mature into active macrophages, which then ingest modified lipoprotein particles, ending up as fat-laden foam cells. Smooth muscle cells in the intima divide, and other smooth muscle cells migrate into the intima from the media attracted by cytokines. Smooth muscle cells then elaborate extracellular matrix, promoting extracellular matrix accumulation in the *growing* atherosclerotic plaque. In later stages, a (thin) fibrous cap, composed primarily of extracellular matrix proteins such as elastin and collagen (Virmani et al., 2000), may form over a large lipid pool. This is the typical morphological structure of vulnerable plaques associated with rupture. Later, for example, inflammatory substances secreted by the tissue can cause the thin fibrous cap to become highly stressed, and possibly rupture, releasing material which can lead to potentially lethal blood clots. Excellent overviews of the current thinking in the medical community pertaining to the growth and rupture of atherosclerotic plaques are provided in Shah (1997), van der Wal and Becker (1999), Chyu and Shah (2001) and Libby (2001a, b), among others.

Corresponding laboratory tests to investigate the biological processes mentioned above are extremely difficult, even though the individual events are relatively straightforward to describe from the mechanical point of view. Physical and numerical modeling of individual portions of this process have been undertaken by numerous researchers, one example is the modeling of the highly nonlinear deformation mechanisms and stress distributions in healthy and diseased arteries under different loading conditions, see, for example, the studies (Holzapfel et al., 2000, 2002a, b) by Holzapfel and co-workers, or the more general overview given by Humphrey (2002) and Holzapfel and Ogden (2003), among others. However, while there are numerous researches detailing specific clinical events involved in the growth and rupture of atherosclerotic plaques, to the knowledge of the authors, there appears to be an absence of works which focuses attention on developing a comprehensive mathematical model, which both addresses all of the events simultaneously and provides robust solutions.

It was the objective of this research to develop a constitutive and computational framework, which assembles very simple models governing essentially different physical events, in order to describe the complex coupled events of atherosclerotic plaque growth and rupture. Since modeling of these coupled events is rather complex, and there being no framework available which could be used as a basis, the present work aims to provide this larger perspective on the problem. In Section 2 we provide the physical setting, while in Section 3 we present computational aspects required to solve the coupled system of nonlinear equations. The concluding remarks mainly focus attention on the limitations of the presented approach, and attempt to motivate several possible improvements.

2. Phenomenological mathematical idealizations

We start by developing a phenomenological model to describe how the cross-section of the artery, $A = \pi r_{in}^2$ (Fig. 1), changes in response to the presence of an excess of lipids in the intima and the subsequent growth of the tissue due to inflammation associated with the adhesion of monocytes onto the intima wall and penetration therein. The inner radius of the artery is denoted by r_{in}. We assume that the blood contains lipids and monocytes in suspension that are convected along by the blood via drag forces. We consider an incompressible, steady, 1D flow profile, with a constant flow rate $\left(Q_0 = v_0 A_0 = \int_A v \, \mathrm{d}A = Q\right)$, through an artery, given by ($q > 0$)

$$v = v_{\max}\left[1 - \left(\frac{r}{r_{in}}\right)^q\right]. \tag{1}$$

Because the flow rate is constant ($Q_0 = Q$) this implies

$$v_{\max} = \frac{Q_0}{A(1 - [2/q + 2])}. \tag{2}$$

The velocity of a monocyte particle of diameter d (see Fig. 1), which is convected with the fluid near the

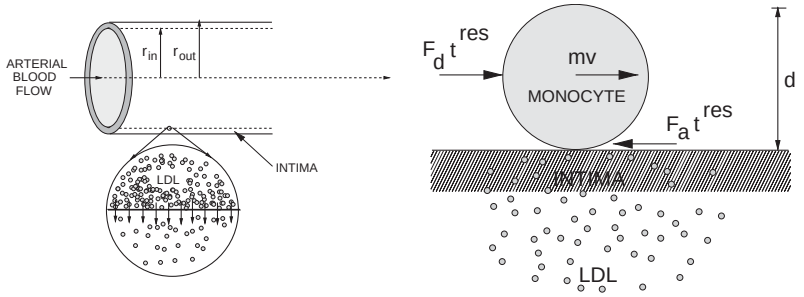

Fig. 1. Schematic for the model problem.

endothelial surface, is approximated by the velocity v^c of its center

$$v^c \stackrel{def}{=} v_{\max}\left[1-\left(\frac{r_{in}-(d/2)}{r_{in}}\right)^q\right]. \tag{3}$$

To determine the critical velocity of the monocyte, v^* say, below which a particle will become arrested at the wall surface, we write an impulse-momentum balance (see Fig. 1)

$$mv^* + \int_0^{t^{res}} \sum F \,\mathrm{d}t \approx mv^* + F_d t^{res} - F_a t^{res} = 0, \tag{4}$$

where m is the mass of the monocyte, and F_d is the drag force imposed on the particle by the fluid, which, for low Reynolds numbers is $F_d \approx 3\pi\mu v^* d$ (law of Stokes), with μ being the absolute viscosity of the fluid. We assume that the adhesive force F_a is proportional to the cross-sectional area of the monocyte, and proportional to the adhesion stress τ_a, i.e. adhesive force per unit area, produced on the intima surface upon contact. We write $F_a \approx \gamma_1 \tau_a \pi d^2/4$, where γ_1 is a constant of proportionality, which scales the contact area to the cross-sectional area of the particle, and t^{res} is the contact time, commonly referred to in the literature as the 'residence time' (see, for example, Libby, 2001a, b). In addition, we assume that $v^* \approx \gamma_2 d/t^{res}$, where γ_2 is another constant of proportionality, which scales the contact time to the critical velocity of the monocyte. The mass of the monocyte is $m = \rho_m \pi d^3/6$, where ρ_m is the reference mass density of the monocyte particle. Substitution into the impulse-momentum balance yields an explicit equation for the critical velocity of the monocyte, i.e.

$$(v^*)^2 + \frac{18\gamma_2\mu v^*}{d\rho_m} - \frac{3\gamma_1\gamma_2\tau_a}{2\rho_m} = 0 \tag{5}$$

which yields

$$v^* = -\frac{9\gamma_2\mu}{d\rho_m} \pm \sqrt{\frac{81\gamma_2^2\mu^2}{d^2\rho_l^2} + \frac{3\gamma_1\gamma_2\tau_a}{2\rho_m}}, \tag{6}$$

where the positive root is the physically correct one. It is assumed that the concentration of the monocytes arrested at the wall, denoted as c_w, is proportional to the difference between the velocity of the monocytes v^c and the critical velocity v^*. Thus,

$$c_w \propto \max\left(0, 1-\frac{v^c}{v^*}\right) \stackrel{def}{=} \eta. \tag{7}$$

As the velocity increases, particles are less likely to adhere, until a critical velocity is met, where no particles adhere. Essentially, one can interpret η as a distribution function, which indicates the likelihood of a particle adhering to the intima surface as a function of the near-wall velocity.

The assumption is now made, that the growing thickness of the intima, denoted as a, is related to the concentration of monocytes by

$$\dot{a} = \mathscr{F}(\eta, \ldots, \text{material parameters}). \tag{8}$$

This phenomenological model accounts for the intimal thickening due to the presence of the monocytes and subsequent reactions due to monocytes and macrophages, etc. Specifically, this takes the form of a somewhat standard growth law, commonly used in analyses of scale growth in pipe flow (see, for example, Fontana, 1986; Shackelford, 2000)

$$\dot{a} = K\eta, \tag{9}$$

where K is a growth rate constant. If η were time-invariant, then the growth would be 'linear' of the form

$$a(t) = K\eta t + a(0). \tag{10}$$

However, this observation can only be taken qualitatively, because η is a function of a and t, due to the fact that v is a function of $r_{in}(t) = r_{out} - a(t)$ (see Fig. 1). In Section 3, we provide an algorithm to solve this coupled system.

In order to describe the rupture of the thin fibrous cap, which is coupled with the growth, we use a simple constitutive approach, and split the stored energy Ψ into purely isochoric ($\bar{\Psi}$) and volumetric (U) parts, i.e.

$$\Psi = \bar{\Psi} + \underbrace{\frac{\kappa}{2}(J-1)^2}_{\stackrel{def}{=} U}, \tag{11}$$

where κ is the bulk modulus of the material, and $J = det\, \boldsymbol{F}$ is the Jacobian determinant of the deformation gradient $\boldsymbol{F} = \nabla_X \boldsymbol{x}$, whereby $\boldsymbol{u} = \boldsymbol{x} - \boldsymbol{X}$ is the displacement vector, and $\boldsymbol{X}$ and $\boldsymbol{x}$ indicate referential position and spatial position of a point relative to a fixed origin. For the associated kinematics, see, for example, Holzapfel (2000).

With $\boldsymbol{C} = \boldsymbol{F}^{\mathrm{T}}\boldsymbol{F}$ denoting the right Cauchy–Green tensor, it is straightforward to derive the stress relation. In particular, the Cauchy stress tensor $\boldsymbol{\sigma}$ is obtained from Ψ through the relation $\boldsymbol{\sigma} = J^{-1}\boldsymbol{F}(2\partial\Psi/\partial\boldsymbol{C})\boldsymbol{F}^{\mathrm{T}}$, (Holzapfel, 2000), and by considering the particular constitutive assumption (11) we get $\boldsymbol{\sigma} = \overline{\boldsymbol{\sigma}} + p\boldsymbol{1}$, where $\overline{\boldsymbol{\sigma}} = J^{-1}\boldsymbol{F}(2\partial\bar{\Psi}/\partial\boldsymbol{C})\boldsymbol{F}^{\mathrm{T}}$ denotes the purely isochoric contribution, and $p\boldsymbol{1}$ the purely volumetric contribution to the stresses, with

$$p = \frac{\partial U}{\partial J} = \kappa(J-1). \tag{12}$$

Note that $p = tr\,\boldsymbol{\sigma}/3$ can be identified as the hydrostatic pressure. Further, we propose that rupture in the thin fibrous cap occurs when the pressure p in the cap exceeds some critical value p^* at a continuum particle, $p \geqslant p^*$ say.[1] We now consider a problem with the simple kinematics, as shown in Fig. 2. Thereby, a continuum particle on the endothelial surface, with referential

[1] The pressure criterion is a logical choice, since it is believed that rupture occurs when the thin fibrous plaque cap, which is essentially a thin membrane, bursts, in a similar manner as an overpumped balloon. The material in the intima is then released, leading to a stroke.

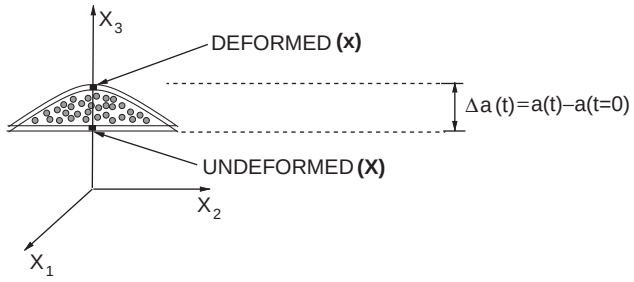

Fig. 2. Continuum particle on the endothelial surface with referential position $\boldsymbol{X}$ displaced to the current position $\boldsymbol{x}$, with $u_1 = u_2 = 0$ and $u_3 = \Delta a(t) X_3$.

position $\boldsymbol{X}$ (with referential coordinates (X_1, X_2, X_3)), is displaced to the current position $\boldsymbol{x}$ (with spatial coordinates (x_1, x_2, x_3)) so that $u_1 = u_2 = 0$ and $u_3 = \Delta a(t) X_3$, with $\Delta a(t) = a(t) - a(t=0)$, are the Cartesian components of the displacement vector $\boldsymbol{u}$. Hence, the matrix representation $[\boldsymbol{F}]$ of the deformation gradient $\boldsymbol{F}$ and the volume ratio J reduces to

$$[\boldsymbol{F}] = \begin{bmatrix} 1 & 0 & 0 \\ 0 & 1 & 0 \\ 0 & 0 & \Delta a(t) + 1 \end{bmatrix},$$

$$J = det[\boldsymbol{F}] = \Delta a(t) + 1, \tag{13}$$

which leads, with Eq. (12), to

$$p = \kappa \Delta a(t). \tag{14}$$

Remark. Although the deformation used is relatively simple, it captures the essence of the swelling of the intima. More complicated deformations would be an overkill since they would be still coupled to the simple fluid model. Furthermore, since the pressure is the only quantity sought after, this deformation is adequate. However, if a more sophisticated rupture criteria would be used, for example involving shear stresses, then the deformation analysis would have to be more detailed.

3. A staggered solution scheme for growth and rupture

To solve the coupled system of equations in the previous section, an implicit fixed-point recursion is used to update the nonlinear velocity-growth coupling within each time step. Given the critical velocity v^* through (6), the procedure at a given time t and with the time increment Δt is as follows:

(I) Solve for fluid velocity (fix $a^i(t) = r_{out} - r^i_{in}(t)$):

$$v^{c,i+1}(t) = v^i_{\max}\left[1 - \left(\frac{r^i_{in}(t) - (d/2)}{r^i_{in}(t)}\right)^q\right]$$

$$\Rightarrow \text{update} : \eta^{i+1}(t) = \max\left(0, 1 - \frac{v^{c,i+1}(t)}{v^*}\right);$$

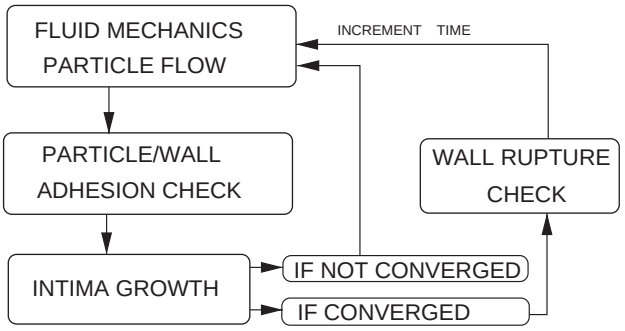

Fig. 3. Schematic flowchart.

(II) Solve for growth (fix $v^{c,i+1}(t)$):

$$\dot{a}^{i+1}(t) = K\eta^{i+1} \Rightarrow a^{i+1}(t) = K\eta^{i+1}\Delta t + a(t - \Delta t)$$

$$\Rightarrow \text{update} : r^{i+1}_{in}(t) = r_{out} - a^{i+1}(t);$$

$$\text{(III) Repeat until} : \|r^{i+1}_{in}(t) - r^i_{in}(t)\| \leqslant TOL. \tag{15}$$

The index of iteration at time t is denoted by $i = 1, \ldots, N$. The first step starts at fixed thickness a of the intima. The fluid mechanical problem is solved for the velocity v^c of the center of the monocyte, and thereafter the particle/wall adhesion check is performed—the distribution function η is computed. In a second step, at fixed velocity v^c, the evolution equation for intimal growth is solved for a, and thereafter r_{in} is computed. This two-step algorithm is continued as long as $\|r^{i+1}_{in}(t) - r^i_{in}(t)\| \leqslant TOL$, where TOL is a small tolerance value. After the process has converged at t, the failure criterion $p(t) \geqslant p^*$ is checked. A schematic flowchart is presented in Fig. 3. Increased accuracy is acquired for smaller time increments Δt in the growth law.

3.1. General convergence criteria

The convergence to a fixed-point solution, as described in scheme (15), is also controlled by the time increment Δt. Thus, during the simulations, if the time step solution does not converge within a certain number of iterations, the time step is reduced.[2] In abstract terms, consider $\mathscr{D}(r_{in}(t)) = \mathscr{F}$, where $r_{in}(t)$ is to be solved for at time t. It is convenient to write an operator split

$$\mathscr{D}(r_{in}(t)) - \mathscr{F} = G(r_{in}(t)) - r_{in}(t) + z = 0, \tag{16}$$

where z is the remainder term in the operator split. A straightforward, well established, type of iterative scheme is

$$r^i_{in}(t) = G(r^{i-1}_{in}(t)) + z, \tag{17}$$

where $i = 1, \ldots, N$ is the index of iteration at time t. The convergence of such a scheme is dependent on the

[2] In addition to convergence issues, for accurate numerical solutions such approaches require small time steps, primarily because the staggering error accumulates with each successive increment.

behavior of G. Namely, a sufficient condition for convergence is that G is a contraction mapping for all $r_{in}^{i}(t)$. Accordingly, we define the error as $e^{i}(t) = r_{in}^{i}(t) - r_{in}(t)$. A necessary restriction for convergence is iterative self-consistency, i.e. the exact solution must be represented by the scheme $G(r_{in}(t)) + z = r_{in}(t)$. Enforcing this restriction, a sufficient condition for convergence is the existence of a contraction mapping

$$|e^{i}(t)| = |r_{in}^{i}(t) - r_{in}(t)| = |G(r_{in}^{i-1}(t)) - G(r_{in}(t))| \leqslant \lambda |r_{in}^{i-1}(t) - r_{in}(t)|, \quad (18)$$

where λ denotes the fixed-point constant. If $0 \leqslant \lambda < 1$ for each iteration i, then $e^{i}(t) \to 0$ for any arbitrary starting value $r_{in}^{i=0}(t)$ as $i \to \infty$. The type of contraction condition discussed is sufficient, but not necessary, for convergence. For more details see, for example, Ostrowski (1966), Ortega and Rockoff (1966), Kitchen (1966), Ames (1977) or Axelsson (1994).

3.2. Qualitative behavior

The fixed-point constant λ may be determined *explicitly* in terms of the material parameters and flow rates involved. This is achieved by collapsing all of the equations into a single one involving the primary variable $r_{in}(t)$ (for convenience, we will omit subsequently the index of iteration at time t). By referring to (15), during the staggering process, we find, by defining $a_0 = a(t - \Delta t)$ and $g(r_{in}(t)) = v^{c}(t)/v^{*}$, that $a(t) = K\eta\Delta t + a_0$. This implies

$$r_{in}(t) = r_{out} - K\eta\Delta t - a_0 = G(r_{in}(t)) + z, \quad (19)$$

in which the definitions

$$G(r_{in}(t)) = K\Delta t g(r_{in}(t)), \quad z = r_{out} - a_0 - K\Delta t \quad (20)$$

are to be used. In this case, with Eqs. (1), (2) and(6) we find that

$$G(r_{in}(t)) = K\Delta t \frac{Q_0/(\pi r_{in}^{2}(t)(1 - (2/q + 2)))[1 - (r_{in}(t) - d/2/r_{in}(t))^{q}]}{-(9\gamma_2\mu/d\rho_m) + \sqrt{(81\gamma_2^{2}\mu^{2}/d^{2}\rho_l^{2}) + (3\gamma_1\gamma_2\tau_a/2\rho_m)}}. \quad (21)$$

Therefore, we have the following observations:

- As either ρ_m, d, Q_0, K or Δt increase, then $G(r_{in}(t))$ increases, thus impairing convergence,
- As either τ_a, μ or q decrease, then $G(r_{in}(t))$ increases, thus impairing convergence.

Eq. (21) allows an explicit expression for the necessary time step Δt to achieve convergence. We obtain

$$K\Delta t \frac{Q_0/(\pi r_{in}^{2}(t)(1 - 2/(q + 2)))[1 - (r_{in}(t) - (d/2)/r_{in}(t))^{q}]}{-9\gamma_2\mu/d\rho_m + \sqrt{(81\gamma_2^{2}\mu^{2}/d^{2}\rho_l^{2}) + (3\gamma_1\gamma_2\tau_a/2\rho_m)}} < TOL < 1 \quad (22)$$

which leads to

$$\Delta t < \frac{TOL(-(9\gamma_2\mu/d\rho_m) + \sqrt{(81\gamma_2^{2}\mu^{2}/d^{2}\rho_l^{2}) + (3\gamma_1\gamma_2\tau_a/2\rho_m)})}{KQ_0/(\pi r_{in}^{2}(t)(1 - 2/(q + 2)))[1 - (r_{in}(t) - (d/2)/r_{in}(t))^{q}]}. \quad (23)$$

3.3. Approximate critical time to rupture

Here we approximate the critical time, t^{*} say, at which rupture occurs. This approximation is based on the premise that rupture depends solely on some critical value p^{*} of the hydrostatic pressure at a continuum particle.

For the rupture criterion to be met, we have $p = p^{*}$, where the particularized form for the hydrostatic pressure is given (14), i.e. $p = \kappa\Delta a(t)$. To find the critical growth we invert this expression, which gives

$$\Delta a(t^{*}) = \frac{p^{*}}{\kappa}. \quad (24)$$

By considering the case where η is slowly varying, thus $\eta \approx (v^{*} - v^{c})/v^{*}$, this leads to an explicit expression for t^{*}. From (10) we find with $\Delta a(t^{*}) = a(t^{*}) - a(0)$ that

$$a(t^{*}) \approx K\eta t^{*} + a(0) \quad \Rightarrow \quad t^{*} = \frac{\Delta a(t^{*})}{K\eta}. \quad (25)$$

Using (24) we then get the critical time

$$t^{*} = \frac{p^{*}}{\kappa K\eta} \quad (26)$$

at which rupture occurs.

3.4. Numerical example

In the following, a specific numerical example is briefly presented with the goal of showing the evolution of certain quantities with time obtained from the solution of the coupled velocity-growth model, as described in this section. In particular, the geometry of the artery and the material parameters used are shown in Table 1 (Berger, 1996). The only constant that was not obtained from the literature was K. This constant was estimated from known approximate times ($\approx$ 15–20 years) to rupture. Therefore, one can consider such a simulation as the result of an inverse problem where K was sought. The constants of proportionality, γ_1 and γ_2, were set to unity and a quadratic velocity profile was used ($q = 2$).

Fig. 4 shows the evolution of the inner radius r_{in} of the artery, the velocity v^{c} of the center of the monocyte, and the pressure p with time t. Under the conditions simulated the atherosclerotic plaque would rupture in $t^{*} = 16$ years. During this process, the inner radius decreases to approximately two-thirds of its original

Table 1
The material parameters used in the simulation

r_{out}	r_{in} $(t=0)$	v_0	K	μ
2.85×10^{-3} m	2.75×10^{-3} m	10^{-1} m/s	10^{-12} m/s	3.5×10^{-3} Ns/m^2
ρ_m	p^*	d	τ_a	κ
8.8×10^2 kg/m^3	10^7 N/m^2	10^{-6} m	10^3 N/m^2	10^{10} N/m^2

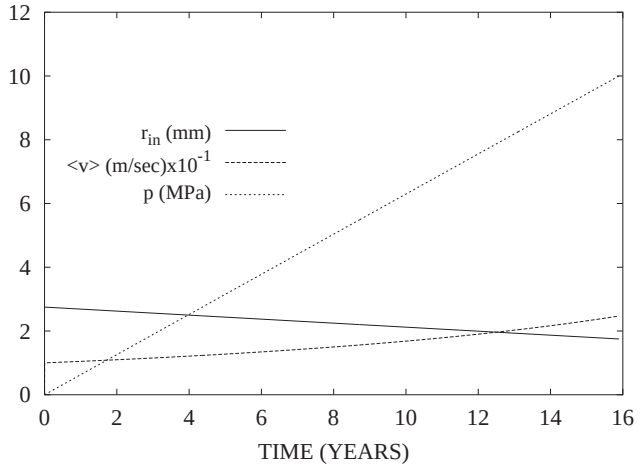

Fig. 4. Time-dependent behavior of the inner radius r_{in} of the artery, the mean flow velocity and the evolution of the pressure p in the thin plaque cap. The rupture limit was set to 10 Mpa. The velocity profile was set to $q = 2$.

value, thus leading to an increased mean velocity of the flow, due to the constant mass flow condition and a decreasing lumen cross-sectional area. Simulation times were on the order of one second on a standard Unix workstation. The analytical approximate estimate in Eq. (26) indicates time to rupture to within 1% of the computed result. The accuracy of the prediction can be attributed to the weakly nonlinear growth.

4. Concluding remarks

This communication is a first attempt to model the overall, long-time coupled phenomena of atherosclerotic plaque growth and rupture from a biomechanical (physical) and numerical point of view. Our long-term goal is to be able to deduce, via inverse biomechanical and biochemical simulation of the temporal evolution and rupture of (vulnerable) atherosclerotic plaques, those characteristics which make them vulnerable. While the overall computational framework developed in this work potentially is general enough for this goal to be attainable, each of the described components of the associated processes should be replaced by more sophisticated models incorporating and capturing more detailed geometrical, physical, and biochemical information. For example, plaque vulnerability is thought to be highly dependent upon the morphology, i.e. 3D geometry and composition, of the domain of interest. In this work the rupture of the plaque is restricted to pressure-based failure. A more sophisticated fracture criterion should also include shear stresses and damage mechanisms.

Realistic assessment of vulnerable atherosclerotic plaques requires advanced (physical) modeling in the following areas:

1. 3D 'morpho-mechanical' data coming from, for example, optical coherence tomography (Yabushita et al., 2002), or high-resolution magnetic resonance imaging (see, for example, Fuster, 2002; Holzapfel et al., 2002b);
2. residence time t^{res} for the monocytes in the intima and its correlation to the concentration at the inner wall boundary;
3. mass transfer of the LDLs into the intima;
4. mechanobiological reactions caused within the intima resulting in the growth of the atherosclerotic plaque; and
5. the failure of the atherosclerotic plaque,

among several other aspects.

More detailed analyses have do be performed in 3D and will inevitably require numerical discretization, employing techniques such as the finite element method. In Zohdi (2002), a recursive staggering strategy which allowed the adaptive control of time step sizes, was developed for large-scale multifield staggered computation of the environmental degradation of micro-heterogeneous structural materials, which could possibly be used in conjunction with more advanced models of atherosclerotic plaque growth and rupture. A powerful staggered solution technique in conjunction with more advanced biomechanical *and* biochemical models in 3D may be helpful in providing a basis for an improved understanding of the interaction of plaque morphology, composition, inflammation, mechanical factors and plaque rupture, potentially enabling predictions for the onset of acute cardiovascular syndromes such as myocardial infarction or stroke. Computational mechanics may provide significant contributions for the

understanding, identification and treatment of vulnerable plaques. This task is being currently pursued by the authors.

References

Ames, W.F., 1977. Numerical Methods for Partial Differential Equation, 2nd Edition. Academic Press, New York.

Axelsson, O., 1994. Iterative Solution Methods. Cambridge University Press, Cambridge.

Berger, S.A., 1996. Physiological fluid mechanics. In: Berger, S.A., Goldsmith, E.W., Lewis, E.R. (Eds.), Introduction to Bioengineering, 1st Edition. Oxford University Press, Oxford, pp. 133–170.

Chyu, K.Y., Shah, P.K., 2001. The role of inflammation in plaque disruption and thrombosis. Rev. Cardiovasc. Med. 2, 82–91.

Davies, M.J., Richardson, P.D., Woolf, N., Katz, D.R., Mann, J., 1993. Risk of thrombosis in human atherosclerotic plaques: role of extracellular lipid, macrophage, and smooth muscle cell content. Br. Heart J. 69, 377–381.

Fontana, M., 1986. Corrosion Engineering. McGraw-Hill, New York.

Fuster, V. (Ed.), 2002. Assessing and Modifying the Vulnerable Atherosclerotic Plaque. Futura Publishing Company, Armonk.

Holzapfel, G.A., 2000. Nonlinear Solid Mechanics. A Continuum Approach for Engineering. Wiley, Chichester.

Holzapfel, G.A., Ogden, R.W. (Eds.), 2003. Biomechanics of Soft Tissue in Cardiovascular Systems. Springer, Wien, New York.

Holzapfel, G.A., Gasser, T.C., Ogden, R.W., 2000. A new constitutive framework for arterial wall mechanics and a comparative study of material models. J. Elasticity 61, 1–48.

Holzapfel, G.A., Gasser, T.C., Stadler, M., 2002a. A structural model for the viscoelastic behavior of arterial walls: continuum formulation and finite element analysis. Eur. J. Mech. A/Solids 21, 441–463.

Holzapfel, G.A., Stadler, M., Schulze-Bauer, C.A.J., 2002b. A layer-specific three-dimensional model for the simulation of balloon angioplasty using magnetic resonance imaging and mechanical testing. Ann. Biomed. Eng. 30, 753–767.

Humphrey, J.D., 2002. Cardiovascular Solid Mechanics. Cells, Tissues, and Organs. Springer, New York.

Kitchen, J., 1966. Concerning the convergence of iterates to fixed points. Studia Math. 27, 247–249.

Libby, P., 2001a. Current concepts of the pathogenesis of the acute coronary syndromes. Circulation 104, 365–372.

Libby, P., 2001b. The vascular biology of atherosclerosis. In: Braunwald, E., Zipes, D.P., Libby, P. (Eds.), Heart Disease. A Textbook of Cardiovascular Medicine, 6th Edition. W.B. Saunders Company, Philadelphia, pp. 995–1009 (Chapter 30).

Libby, P., Aikawa, M., 2002. Stabilization of atherosclerotic plaques: new mechanisms and clinical targets. Nat. Med. 8, 1257–1262.

Loree, H.M., Kamm, R.D., Stringfellow, R.G., Lee, R.T., 1992. Effects of fibrous cap thickness on peak circumferential stress in model atherosclerotic vessels. Circ. Res. 71, 850–858.

Ortega, J., Rockoff, M., 1966. Nonlinear difference equations and gauss-seidel type iterative methods. SIAM J. Numer. Anal. 3, 497–513.

Ostrowski, A., 1966. Solution of Equations and Systems of Equations. Academic Press, New York.

Richardson, P.D., Davies, M.J., Born, G.V.R., 1989. Influence of plaque configuration and stress distribution on fissuring of coronary atherosclerotic plaques. Lancet 2 (8669), 941–944.

Shackelford, J.F., 2000. Material Science for Engineers, 5th Edition. Prentice-Hall, Englewood Cliffs, NJ.

Shah, P.K., 1997. Plaque disruption and coronary thrombosis: new insight into pathogenesis and prevention. Clin. Cardiol. 20 (Suppl. II), II–38–II-44.

Virmani, R., Kolodgie, F.D., Burke, A.P., Farb, A., Schwartz, S.M., 2000. Lessons from sudden coronary death: a comprehensive morphological classification scheme for atherosclerotic lesions. Arterioscl. Thromb. Vasc. Biol. 20, 1262–1275.

van der Wal, A.C., Becker, A.E., 1999. Atherosclerotic plaque rupture—pathologic basis of plaque stability and instability. Cardiovasc. Res. 41, 334–344.

Yabushita, H., Bouma, B.E., Houser, S.L., Aretz, H.T., Jang, I.K., Schlendorf, K.H., Kauffman, C.R., Shishkov, M., Kang, D.H., Halpern, E.F., Tearney, G.J., 2002. Characterization of human atherosclerosis by optical coherence tomography. Circulation 106, 1640–1645.

Zohdi, T.I., 2002. An adaptive–recursive staggering strategy for simulating multifield coupled processes in microheterogeneous solids. Int. J. Numer. Meth. Engr. 53, 1511–1532.